ADVANCES IN ATMOSPHERIC SCIENCES, VOL. 35, MAY 2018, 531–539

• **Original Paper** •

Vortex Rossby Waves in Asymmetric Basic Flow of Typhoons

Tianju WANG[1], Zhong ZHONG*[1,2], and Ju WANG[1]

[1] *College of Meteorology and Oceanography, National University of Defense Technology, Nanjing* 211101*, China*

[2] *Jiangsu Collaborative Innovation Center for Climate Change, Nanjing University, Nanjing* 210023*, China*

(Received 31 May 2017; revised 19 September 2017; accepted 24 October 2017)

ABSTRACT

Wave ray theory is employed to study features of propagation pathways (rays) of vortex Rossby waves in typhoons with asymmetric basic flow, where the tangential asymmetric basic flow is constructed by superimposing the wavenumber-1 perturbation flow on the symmetric basic flow, and the radial basic flow is derived from the non-divergence equation. Results show that, in a certain distance, the influences of the asymmetry in the basic flow on group velocities and slopes of rays of vortex Rossby waves are mainly concentrated near the radius of maximum wind (RMW), whereas it decreases outside the RMW. The distributions of radial and tangential group velocities of the vortex Rossby waves in the asymmetric basic flow are closely related to the azimuth location of the maximum speed of the asymmetric basic flow, and the importance of radial and tangential basic flow on the group velocities would change with radius. In addition, the stronger asymmetry in the basic flow always corresponds to faster outward energy propagation of vortex Rossby waves. In short, the group velocities, and thereby the wave energy propagation and vortex Rossby wave ray slope in typhoons, would be changed by the asymmetry of the basic flow.

Key words: asymmetric basic flow, vortex Rossby waves, group velocity, propagation pathways, wave ray

Citation: Wang, T. J., Z. Zhong, and J. Wang, 2018: Vortex Rossby waves in asymmetric basic flow of typhoons. *Adv. Atmos. Sci.*, **35**(5), 531–539, https://doi.org/10.1007/s00376-017-7126-y.

1. Introduction

Observations have shown that when a tropical cyclone reaches a certain intensity, pronounced spiral cloud bands outside the eye wall of the tropical cyclone are formed (Huang and Chao, 1980). Such spiral clouds are expected to grow along the radial direction and rotate around the typhoon center at a velocity not equal to the velocity of the basic flow (Liu and Yang, 1980). Distinct wave-like fluctuations can be observed in the spiral cloud bands, indicating the existence of waves and eddies in the typhoon vortex (MacDonald, 1968; Yu, 2002).

Studies of wave structures in typhoons can be traced back to the 1940s, when it was found that the spiral cloud bands of typhoons exhibit many features similar to inertia-gravity waves in the shallow water model. These wave structures in typhoons could be well explained by gravity wave theory (Wexler, 1947; Tepper, 1958; Tatehira, 1961). Huang and Chao (1980) indicated that the group velocity of inertia-gravity waves in typhoons was about 90 km h^{-1}, and Liu and Yang (1980) found that the average phase velocity of inertia-gravity waves (C_0) was 28 m s^{-1}. Niu (1991) argued that inertia-gravity waves in an unstable condition is a key factor that determines the development of typhoons. Anthes (1972) and Kurihara (1976) simulated tropical cyclones and found that energy in typhoons is largely dissipated in the form of gravity waves. However, despite great progress in the study of typhoons with the theory of inertia-gravity waves, one critical weakness in the application of gravity wave theory for typhoon studies is that the theoretical propagation velocity of inertia-gravity waves is much faster than the observed moving speed of typhoon spiral cloud bands (Yu, 2002). Thereby, it is necessary to seek other more reasonable explanations for the wave structures in typhoons.

As early as in the late 1960s, MacDonald (1968) found that wave structures similar to planetary Rossby waves exist in typhoons, which are actually the vortex Rossby waves proposed later by Montgomery and Kallenbach (1997). The theory of vortex Rossby waves overcomes the weakness of classical inertia-gravity wave theory, and yields a theoretical wave propagation velocity that is the same as in observations (Yu, 2002). Shen et al. (2007) investigated vortex Rossby waves in both barotropic and baroclinic fluids, and their results indicated that barotropic and baroclinic vortex Rossby waves could be triggered by second-order horizontal and vertical shears in the basic flow of a typhoon. By studying the topographic impact on planetary Rossby waves, Luo and Chen (2003) investigated the influences of topography on the propagation of vortex Rossby waves using a quasi-

* Corresponding author: Zhong ZHONG
E-mail: zhong_zhong@yeah.net

geostrophic, barotropic model, and proposed the concept of topographic vortex Rossby waves. Deng et al. (2004) studied the effects of the Rossby parameter β in the formation of vortex Rossby waves using scale analysis and found that vortex Rossby waves could be triggered when the Rossby parameter β is introduced into a basic flow that even has no radial shears. Qiu et al. (2010) revealed a significant contribution of vortex Rossby waves to the formation of the secondary eye wall of a typhoon. In addition, based on their study of a typhoon process, Hall et al. (2013) indicated that the vortex Rossby waves with wavenumber-2 and 3 are closely linked with deep convection that develops rapidly in typhoons. Furthermore, wave ray theory has also been applied to study the impact of vortex Rossby waves on energy propagation in typhoons (Zhong et al., 2002).

Many previous studies have studied vortex Rossby waves from various perspectives. However, for simplicity, the basic flow of a typhoon is always assumed to be symmetrical; whereas, in reality, it is often asymmetrical. Due to the asymmetry in the basic flow of a typhoon, the vorticity gradient will change with azimuth angle, which could radically affect the nature of the vortex Rossby waves. Thereby, using an asymmetric typhoon basic flow that is more realistic will be helpful in improving vortex Rossby wave theory and obtaining more representative results. In the present study, based on wave ray theory, a model with an asymmetric typhoon basic flow is employed to discuss the group velocity of vortex Rossby waves and the nature of wave rays.

2. Vortex Rossby waves and rays in asymmetric basic flow of typhoons

Barotropic shallow water equations in the cylindrical coordinate system with the f-plane approximation can be written as (Liu and Liu, 2011)

$$\frac{\partial u}{\partial t}+u\frac{\partial u}{\partial r}+\frac{v\partial u}{r\partial\theta}-\frac{v^2}{r}=-g\frac{\partial h}{\partial r}+f_0 v\,, \tag{1}$$

$$\frac{\partial v}{\partial t}+u\frac{\partial v}{\partial r}+\frac{v\partial v}{r\partial\theta}+\frac{uv}{r}=-g\frac{\partial h}{r\partial\theta}-f_0 u\,, \tag{2}$$

where u is the radial velocity, v is the tangential velocity, r is the radius, θ is the azimuth angle (in radians), h is the height of the free surface, f_0 is the Coriolis parameter, g is the gravitational acceleration, and t represents time.

The dimensionless variables listed below are introduced in the present study:

$$\begin{aligned}(\tilde{u},\tilde{v})&=(u,v)/U_0\\ \tilde{r}&=r/R\\ \Delta\tilde{h}&=\Delta h/\Delta H\\ \tilde{t}&=t/T\\ \tilde{\theta}&=\theta\,,\end{aligned} \tag{3}$$

where U_0 ($\sim 10^1$ m s^{-1}), R ($\sim 10^6$ m), ΔH ($\sim 10^2$ m) and T ($\sim 10^5$ s) are the horizontal velocity, typhoon radius, temporal variability of height on the free surface, and characteristic time, respectively. Substituting the above variables for their corresponding variables in Eqs. (1) and (2), which are then divided by U_0^2/R, we have

$$\lambda\tilde{u}_t+\tilde{u}\tilde{u}_r+\frac{\tilde{v}}{\tilde{r}}\tilde{u}_\theta-\frac{\tilde{v}^2}{\tilde{r}}=-\frac{g\Delta H}{U_0^2}\tilde{h}_r+R_0^{-1}\tilde{v}\,, \tag{4}$$

$$\lambda\tilde{v}_t+\tilde{u}\tilde{v}_r+\frac{\tilde{v}}{\tilde{r}}\tilde{v}_\theta+\frac{\tilde{u}\tilde{v}}{\tilde{r}}=-\frac{g\Delta H}{U_0^2}\tilde{h}_\theta-R_0^{-1}\tilde{u}\,, \tag{5}$$

where $\lambda=R/(TU_0)$, $R_0^{-1}=f_0R/U_0$, and the variable with subscript means taking the derivative of the variable, for example, $\tilde{u}_t=\partial\tilde{u}/\partial t$, $\tilde{u}_r=\partial\tilde{u}/\partial r$. Different values of λ correspond to different typhoon structures. In the present study, the horizontal scale of a typhoon is set to be the scale of large-scale movement, i.e., $R\sim TU_0$; thereby, $\lambda=1$. Assuming $\tilde{v}=\tilde{v}(\tilde{t},\tilde{r},\tilde{\theta})$, $\tilde{u}=\tilde{u}(\tilde{t},\tilde{r},\tilde{\theta})$, and considering the horizontal divergence to be zero, the dimensionless vorticity equation can be derived from Eq. (4) and Eq. (5) (the $\sim$ on the top is omitted) and written as

$$\frac{\partial\zeta}{\partial t}+\frac{v}{r}\frac{\partial\zeta}{\partial\theta}+u\frac{\partial\zeta}{\partial r}=0\,, \tag{6}$$

where $\zeta=v/r+\partial v/\partial r-(1/r)(\partial u/\partial\theta)$.

Assuming $v=\bar{v}(r,\theta)+v'(t,r,\theta)$, $u=\bar{u}(r,\theta)+u'(t,r,\theta)$, both are constructed by basic flow and perturbation flow respectively, and substituting them for u and v in Eq. (6) yields

$$\frac{\partial\zeta'}{\partial t}+\frac{\bar{v}}{r}\frac{\partial\zeta'}{\partial\theta}+\frac{v'}{r}\frac{\partial\bar{\zeta}}{\partial\theta}+\frac{\bar{v}}{r}\frac{\partial\bar{\zeta}}{\partial\theta}+\bar{u}\frac{\partial\zeta'}{\partial r}+u'\frac{\partial\bar{\zeta}}{\partial r}+\bar{u}\frac{\partial\bar{\zeta}}{\partial r}=0\,. \tag{7}$$

Without loss of generality, here, the tangential asymmetric basic flow is constructed by superimposing the wavenumber-1 perturbation flow on the symmetric tangential basic flow (Zhong et al., 2007). The dimensionless tangential asymmetric basic flow can be expressed by

$$\bar{v}=\frac{ar}{1+br^2}[1+\mu\sin(\theta+\theta_0)]\,. \tag{8}$$

With Eq. (8), the radial basic flow $\bar{u}$ can be derived from the non-divergence equation as follows:

$$\bar{u}=-\frac{a}{2br}\ln(1+br^2)[\mu\cos(\theta+\theta_0)]\,, \tag{9}$$

where μ ($\sim 10^{-1}$) is the parameter of asymmetry for the basic flow, a and b are parameters for the basic flow structure, and θ_0 is the initial azimuth of the wavenumber-1 perturbation flow. When μ is set to zero, Eqs. (8) and (9) degenerate into an expression for the symmetric basic flow, and the larger value of μ corresponds to the stronger asymmetry in the basic flow. In addition, the radius of maximum wind (RMW) can be determined by parameters a and b. From Eq. (8), one can yield a value of $b^{-1/2}$ for the RMW. In the present study, we set $a=20$ and $b=100$; then, the corresponding dimensionless RMW is $r=0.1$, which is about 100 km. Moreover, the locations of maximum and minimum velocities in the asymmetric basic flow are determined by the initial azimuth angle θ_0.

Using the dimensional format of Eqs. (8) and (9) (Huang and Chao, 1980) (i.e., multiplied by the characteristic speed

U_0 = 50 m s^{-1}) and specifying the initial azimuth angle $\theta_0 = 0$ and asymmetry intensity parameter $\mu = 0.2$, the distributions of the tangential symmetric basic flow, the tangential wavenumber-1 perturbation flow, the tangential asymmetric basic flow, and the radial basic flow, are shown in Figure 1. It is clear that the tangential asymmetric basic flow speed (Figure 1c) is no longer distributed as concentric circles symmetrical about the typhoon center due to the consideration of the tangential wavenumber-1 perturbation flow (Figure 1b). Instead, large values occur to the north of the typhoon center and the tangential basic flow speed is obviously not symmetric about the typhoon center. When $\mu = 0.2$, the maximum flow speeds in the tangential symmetric basic flow, the tangential wavenumber-1 perturbation flow and the tangential asymmetric basic flow are 50 m s^{-1}, 10 m s^{-1} and 60 m s^{-1}, respectively.

Figure 2 shows the distributions of $\bar{u}(\partial\bar{\zeta}/\partial r) + (\bar{v}/r)(\partial\bar{\zeta}/\partial\theta)$, $(v'/r)(\partial\bar{\zeta}/\partial\theta)$ and $u'(\partial\bar{\zeta}/\partial r)$ in Eq. (7), from which it can be seen that $\bar{u}(\partial\bar{\zeta}/\partial r)+(\bar{v}/r)(\partial\bar{\zeta}/\partial\theta)$ is very small when r is relatively small, but it will increase quickly with r. So, in this study, we assume $\bar{u}(\partial\bar{\zeta}/\partial r)+(\bar{v}/r)(\partial\bar{\zeta}/\partial\theta) \approx 0$ in $r \sim [0, 0.35]$, as it is much smaller than the other items in this range. Moreover, the average tangential and radial speed within the ranges of $r \sim [0, 0.35]$ and $\theta \sim [0, 2\pi]$ in the asymmetric basic flow is 37.5 m s^{-1} and -6.8 m s^{-1}.

Based on the definition of the stream function (ψ), $v = \partial\psi/\partial r$, $u = -(1/r)(\partial\psi/\partial\theta)$, and the vorticity equation, Eq. (7), can be written in linear form in $r \sim [0, 0.35]$:

$$\left(\frac{\partial}{\partial t} + \frac{\bar{v}}{r}\frac{\partial}{\partial\theta} + \bar{u}\frac{\partial}{\partial r}\right)\nabla^2\psi' + \frac{1}{r}\frac{\partial\psi'}{\partial r}\frac{\partial\bar{\zeta}}{\partial\theta} - \frac{1}{r}\frac{\partial\psi'}{\partial\theta}\frac{\partial\bar{\zeta}}{\partial r} = 0\,. \quad (10)$$

The solution to Eq. (10) can be obtained using the Wentzel-Kremers-Brillouin-Jeffreys (WKBJ) method. Suppose the solution to the slowly evolving wave packet (Zhong et al., 2002; Tao et al., 2012) is

$$\psi' = \Psi(R, \Theta, T)e^{i\alpha(r,\theta,t)}\,, \quad (11)$$

where $(R, T, \Theta) = \varepsilon(r, t, \theta)$ and ε is a parameter smaller than 1,

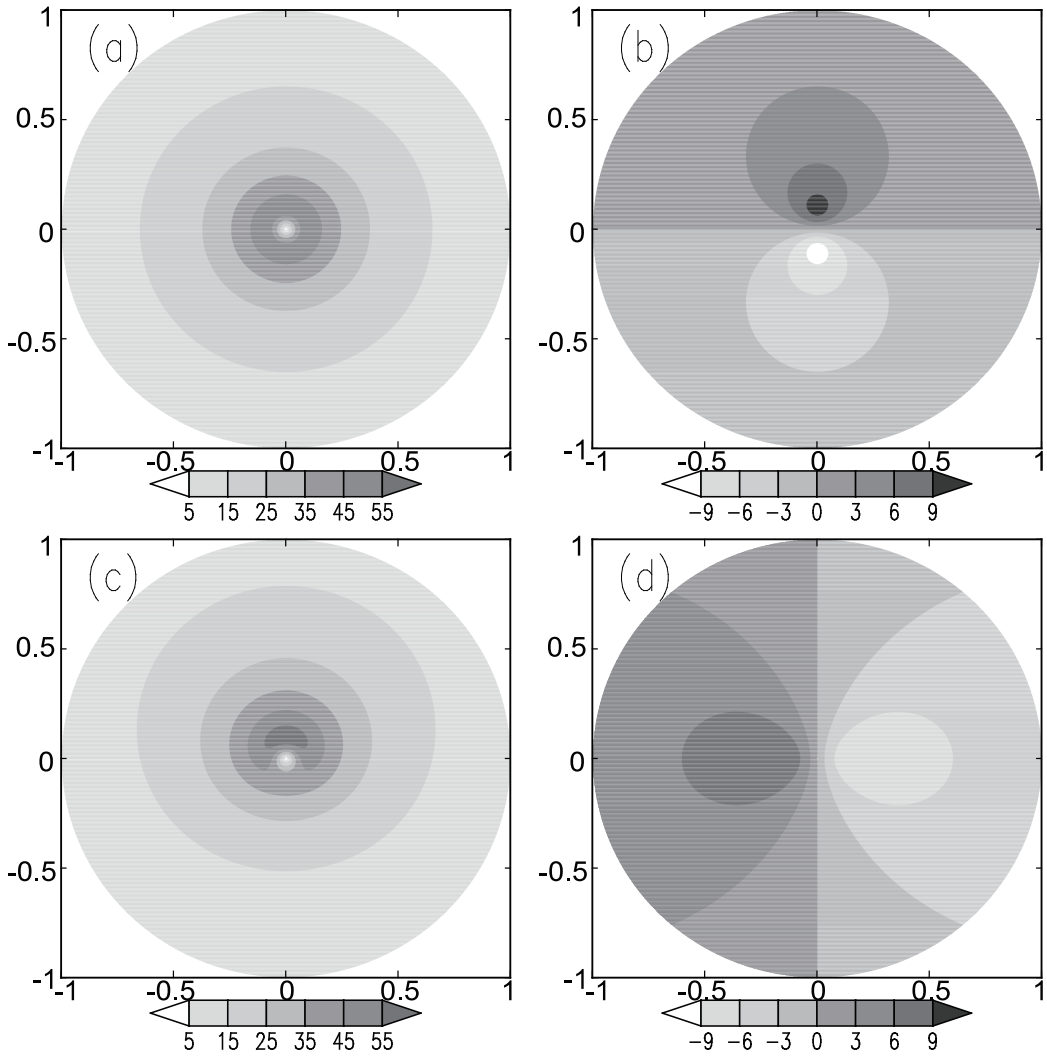

Fig. 1. Distributions of the speed of tangential and radial basic flow (units: m s^{-1}): (a) tangential symmetric basic flow; (b) tangential wavenumber-1 perturbation flow; (c) tangential asymmetric basic flow; (d) radial basic flow (the abscissa and ordinate indicate dimensionless distances from the typhoon center).

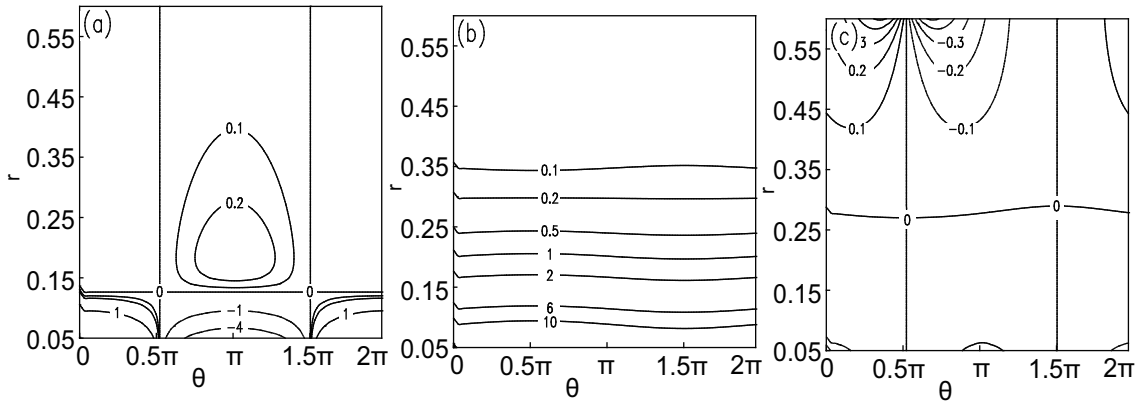

Fig. 2. Distributions of (a) $(v'/r)(\partial\bar{\zeta}/\partial\theta)$, (b) $u'(\partial\bar{\zeta}/\partial r)$ and (c) $\bar{u}(\partial\bar{\zeta}/\partial r)+(\bar{v}/r)(\partial\bar{\zeta}/\partial\theta)$ on the θ–r plane.

we have

$$\begin{aligned}\frac{\partial\psi'}{\partial t} &= \left(\frac{\partial\Psi}{\partial T}\varepsilon - i\omega\Psi\right)e^{i\alpha(r,\theta,t)}\\ \frac{\partial\psi'}{\partial r} &= \left(\frac{\partial\Psi}{\partial R}\varepsilon + \frac{ik}{r}\Psi\right)e^{i\alpha(r,\theta,t)}\\ \frac{\partial\psi'}{\partial\theta} &= \left(\frac{\partial\Psi}{\partial\Theta}\varepsilon + il\Psi\right)e^{i\alpha(r,\theta,t)}\,,\end{aligned} \tag{12}$$

where k and l are radial and tangential wavenumbers, respectively. Substituting Eq. (12) into Eq. (10) and omitting the small term that includes ε, we obtain the frequency equation for vortex Rossby waves:

$$\left(\omega - \frac{\bar{v}}{r}l - \frac{\bar{u}}{r}k\right)\left(\frac{k^2}{r^2}+\frac{l^2}{r^2}\right) - \frac{l}{r}\frac{\partial\bar{\zeta}}{\partial r} + \frac{k}{r^2}\frac{\partial\bar{\zeta}}{\partial\theta} = 0\,, \tag{13}$$

which yields

$$\omega = \left[\frac{\bar{v}}{r}l + \frac{\bar{u}}{r}k + \frac{rl\frac{\partial\bar{\zeta}}{\partial r} - k\frac{\partial\bar{\zeta}}{\partial\theta}}{(k^2+l^2)}\right], \tag{14}$$

where ω is the frequency.

The radial and tangential group velocities, $C_{g,r}$ and $C_{g,\theta}$ Liu and Yang (1980), can be expressed as

$$\begin{aligned}C_{g,r} &= \left[\bar{u} + \frac{r(k^2-l^2)\frac{\partial\bar{\zeta}}{\partial\theta} - 2klr^2\frac{\partial\bar{\zeta}}{\partial r}}{(k^2+l^2)^2}\right],\\ C_{g,\theta} &= \left[\bar{v} + \frac{2klr\frac{\partial\bar{\zeta}}{\partial\theta} + r^2(k^2-l^2)\frac{\partial\bar{\zeta}}{\partial r}}{(k^2+l^2)^2}\right]\end{aligned} \tag{15}$$

$$\frac{dr}{rd\theta} = \frac{C_{g,r}}{C_{g,\theta}}\,. \tag{16}$$

Substituting Eq. (15) into Eq. (16), we can obtain Eq. (17) shown below:

$$\frac{dr}{d\theta} = r\left(\frac{C_{g,r}}{C_{g,\theta}}\right), \tag{17}$$

where $dr/(rd\theta)$ is the slope of the wave ray.

Integration of Eq. (17) can yield the rays of vortex Rossby waves in asymmetric basic flow.

3. Numerical solution of the wave ray equation

Since it is hard to obtain the analytical solution of the wave ray, Eq. (17), here, we seek its solution by numerical integration. The scheme for numerical integration is written as

$$r(n+1) = r(n) + \Delta\theta f(r(n),\theta(n))\,, \tag{18}$$

where n is the number of integration steps, $\Delta\theta$ is the integration step, and $f(r,\theta)$ is the term on the right-hand side of Eq. (17). The initial value $\theta(0)$ is set to zero; the integration range of r is set to $[0,0.35]$; the integration step $\Delta\theta = 0.01$; and wavenumber $k = l = 1$. Figure 3 presents the wave rays obtained by numerical integration under the above conditions when μ is set to 0, 0.2 and 0.3, respectively.

Figure 3 shows that the vortex Rossby wave rays propagate outward in a spiral pattern. The distances from the typhoon center of the wave rays increase with the azimuth

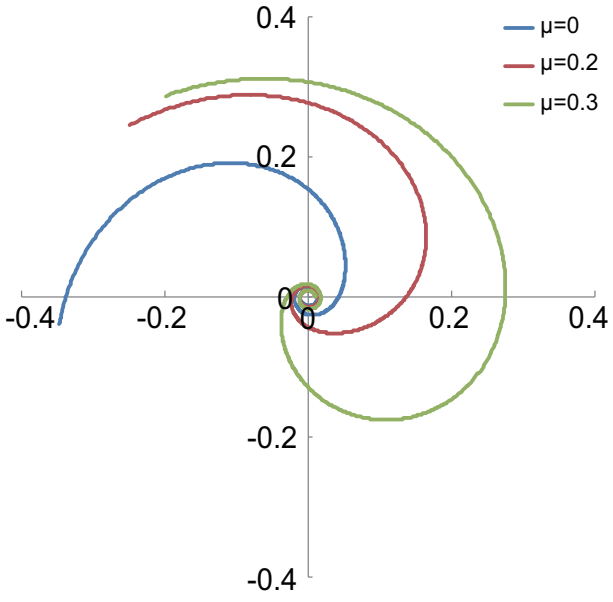

Fig. 3. Wave rays corresponding to various values of μ (the abscissa and the ordinate indicate dimensionless distances from the typhoon center).

angle and, apparently, the differences between the rays increase with the intensity of asymmetry (μ). The larger the value of μ, the greater the increase in the distance of the wave ray, and that makes a wave ray with larger μ farther away from the typhoon center. Although the difference between the asymmetric wave ray and the symmetric one is still large, the difference between wave rays for $\mu = 0.2$ and $\mu = 0.3$ becomes smaller with the increasing of r. This suggests that the impact of the basic flow asymmetry on wave rays will generally decrease and ultimately be constrained within a certain radius.

4. Group velocity

Based on Eq. (17) for wave rays, the radial and tangential group velocities ($C_{g,r}$ and $C_{g,\theta}$) are two important factors affecting wave rays. In the following, we take $\mu = 0.2$ and $\theta_0 = 0$ as an example to explore the impacts of asymmetric basic flow on the vortex Rossby wave rays via analyzing characteristics of the radial and tangential group velocities.

Figure 4 displays the distributions of dimensionless radial group velocity $C_{g,r}$ on the θ–r plane in both symmetric and asymmetric basic flows. In the symmetric basic flow (Fig. 4a), $C_{g,r}$ is always irrelevant to azimuth angle θ and only changes with radius r. The large value of $C_{g,r}$ appears at $r = 0.1$ (where the maximum tangential wind speed appears). In the asymmetric basic flow (Fig. 4b), $C_{g,r}$ changes with both r and θ and the largest value also appears at around $r = 0.1$. The average dimensionless value of $C_{g,r}$ is about 0.50 and the largest is 1.21 within the ranges of $r \sim [0, 0.35]$ and $\theta \sim [0, 2\pi]$, corresponding to an average and maximum radial group velocity of 25 m s^{-1} and 60.5 m s^{-1}. With Eq. (8), it can be found that when $\mu = 0.2$ the dimensionless maximum radial basic flow velocity $\bar{u}$ is -0.16, corresponding to -8.0 m s^{-1}, which is much slower than the maximum $C_{g,r}$. The average dimensionless radial basic flow speed is -0.14, corresponding to the average value of -6.8 m s^{-1}, which is also much slower than the average $C_{g,r}$. When compared with $\bar{v}$, although the average $C_{g,r}$ is smaller, the maximum value of $C_{g,r}$ is almost the same as $\bar{v}$. This indicates that the characteristic of $C_{g,r}$ is identical to that of $\bar{v}$, and the wave energy could propagate outward rapidly.

The difference between radial group velocities in symmetric and asymmetric basic flows can be written as

$$\Delta C_{g,r} = C_{g,r\_\mathrm{asy}} - C_{g,r\_\mathrm{sy}} , \tag{19}$$

where C_{g,r_asy} and C_{g,r_sy} are radial group velocities in symmetric and asymmetric conditions, respectively.

The distribution of $\Delta C_{g,r}$ on the θ–r plane is displayed in Fig. 5, which shows that $\Delta C_{g,r}$ also reaches its maximum at around $r = 0.1$.

It is worth noting that the distributions of $C_{g,r}$ and $\Delta C_{g,r}$ shown in Fig. 4 and Fig. 5 are obtained under the condition of an initial azimuth angle $\theta_0 = 0$ in the tangential wavenumber-1 perturbation flow and the radial basic flow. Compared with Fig. 1, it is easy to identify that $\Delta C_{g,r}$ is affected by both the features of asymmetry in the tangential and radial basic flows. For example, the maximum and minimum values of the wavenumber-1 perturbation flow are located at azimuth angles of $\theta = 0.5\pi$ and 1.5π, and the locations of maximum and minimum values of the radial basic flow are at a $\theta = \pi$ and 0. When r is small, the maximum and minimum values of $\Delta C_{g,r}$ appear at $\theta \approx \pi$ and 2π, which is close to the location of the maximum and minimum values of $\bar{u}$. Whereas, for the larger r, the location of the maximum and minimum values of $\Delta C_{g,r}$ will rotate clockwise and approach those of $\bar{v}$, as shown in Fig. 5. This suggests that both the tangential asymmetric wavenumber-1 flow and the radial basic flow can affect the distribution of radial group velocity $C_{g,r}$; however, the tangential and radial basic flow shows different importance for

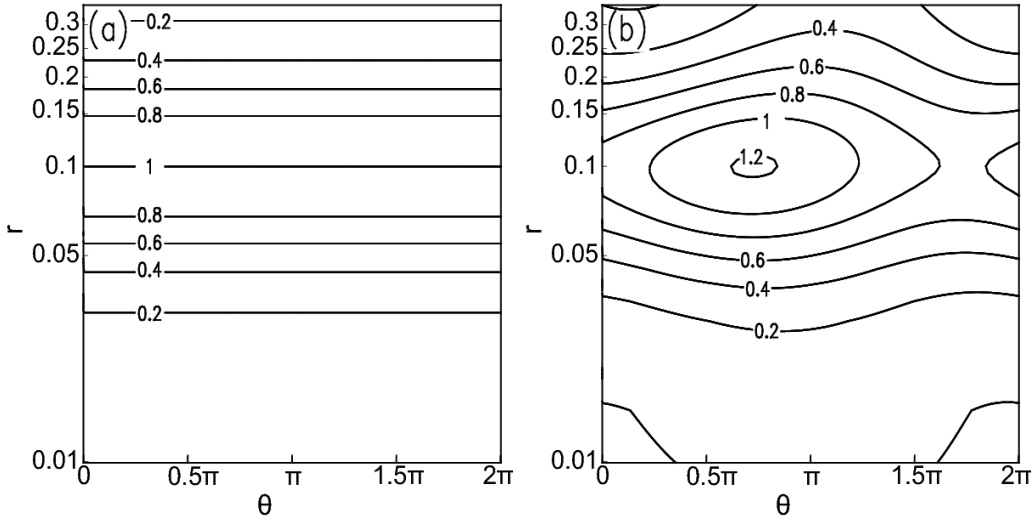

Fig. 4. Distributions of dimensionless radial group velocity $C_{g,r}$ on the θ–r plane in (a) symmetric basic flow and (b) asymmetric basic flow.

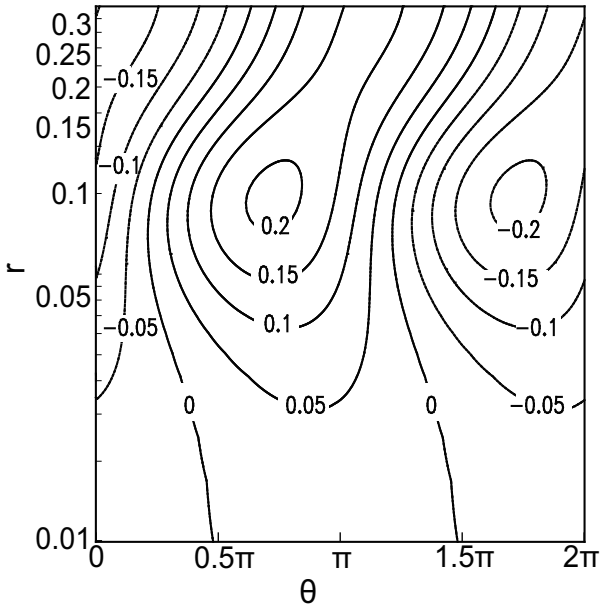

Fig. 5. Distribution of ΔC_{gr} on the θ–r plane.

different r. Generally, the locations of the maximum and minimum value of $\Delta C_{g,r}$ are closely linked with the azimuth angles of the asymmetry. Therefore, if the asymmetries of the basic flows intensify at specific azimuth angles, then $C_{g,r}$ will increase around these angles, and the wave energy will propagate outward more rapidly there. Similarly, when the asymmetry decreases at specific azimuth angles, the wave energy will propagate outward more slowly along these directions.

The distribution of tangential group velocity $C_{g,\theta}$ on the θ–r plane is presented in Fig. 6, which shows that the distribution of $C_{g,\theta}$ (Fig. 6a) in the symmetric basic flow is similar to that of $C_{g,r}$ (Figure 4a), and both change only with radius and reach their maximum values at $r = 0.1$. In the asymmetric basic flow, however, although the maximum values of $C_{g,r}$ and $C_{g,\theta}$ both appear at around $r = 0.1$ (Fig. 6b and Fig. 4b), with little difference in values, $C_{g,\theta}$ is much larger than $C_{g,r}$ at a certain radius (e.g., at $r = 0.3$, $C_{g,r} \approx 0.2$, $C_{g,\theta} \approx 0.6$), indicating that $C_{g,r}$ and $C_{g,\theta}$ are different from each other. $C_{g,r}$ decreases more rapidly along the radial direction, and thereby the speed of wave energy propagation along the radial direction will become slow beyond a certain radius. In contrast, the radial gradient of $C_{g,\theta}$ is relatively small, so the tangential propagation of wave energy can still maintain in regions far away from the typhoon center. It can be estimated that the average value of dimensionless $C_{g,\theta}$ in the region shown in Fig. 6 ($r \sim [0, 0.35], \theta \sim [0, 2\pi]$) is 0.75, which corresponds to 37.5 m s^{-1}, and is just the same as the average value of $\bar{v}$. Whereas, the maximum value of dimensionless $C_{g,\theta}$ is 1.20, corresponding to 60.0 m s^{-1}, which is also the same as the maximum value of $\bar{v}$. This suggests that wave energy can propagate along the tangential direction at the average speed of the tangential basic flow. In short, the wave energy propagation along the tangential direction is much faster than that in the radial direction.

The difference between tangential group velocities in symmetric and asymmetric basic flows ($\Delta C_{g,\theta}$) can be expressed as

$$\Delta C_{g,\theta} = C_{g,\theta\_\mathrm{asy}} - C_{g,\theta\_\mathrm{sy}} , \tag{20}$$

where $C_{g,\theta\_\mathrm{asy}}$ and C_{g,θ_sy} are the tangential group velocities in symmetric and asymmetric basic flows, respectively.

Figure 7 shows the distribution of $\Delta C_{g,\theta}$ on the θ–r plane. $\Delta C_{g,\theta}$ changes with both azimuth angle θ and radius r. The change in $\Delta C_{g,\theta}$ with θ demonstrates the asymmetric feature of tangential wavenumber-1 flow and the radial basic flow, and the azimuth angles corresponding to the locations of asymmetric maximum and minimum values also change with r.

Compared with Fig. 1, it is clear that when r is relatively

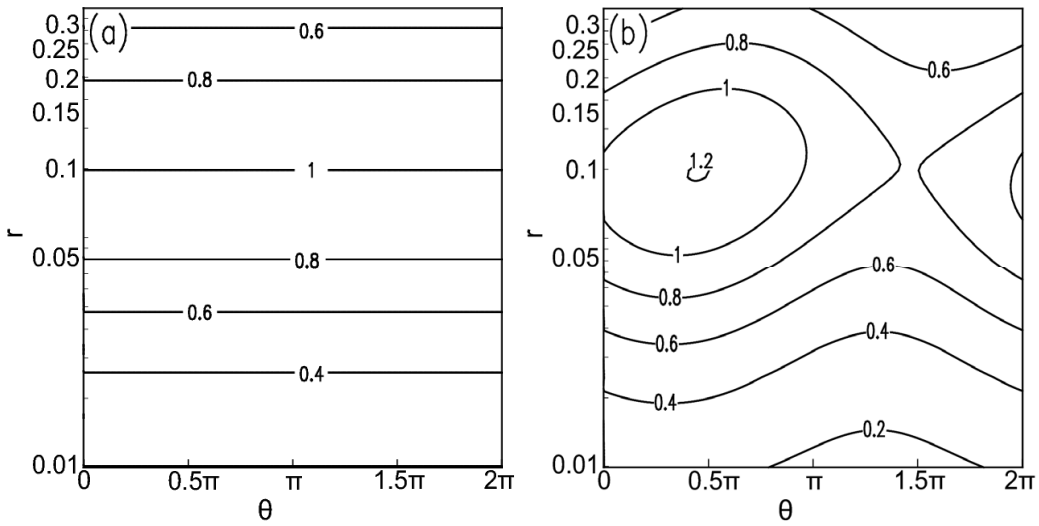

Fig. 6. Distribution of dimensionless tangential group velocity $C_{g,\theta}$ on the θ–r plane in (a) symmetric basic flow and (b) asymmetric basic flow.

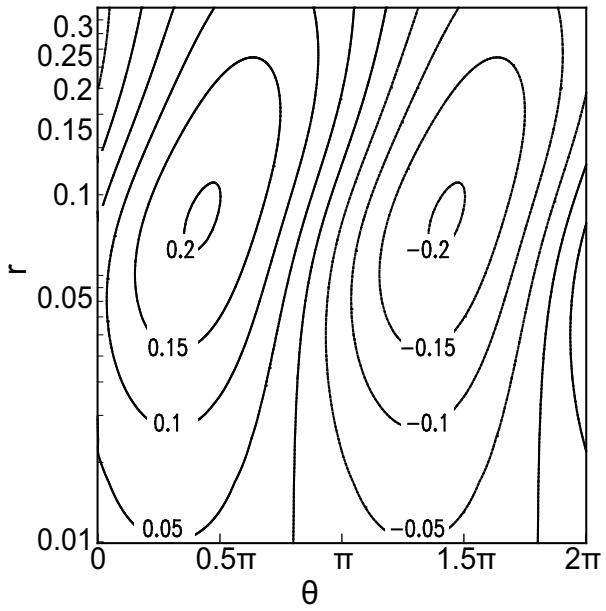

Fig. 7. Distribution of $\Delta C_{g,\theta}$ on the θ–r plane.

small, the large and small values of $\Delta C_{g,\theta}$ are located just between the locations of the maximum and minimum value of $\bar{v}$ and $\bar{u}$ (e.g., when $r \sim [0.01, 0.05]$, the maximum and minimum values of $\Delta C_{g,\theta}$ are located at about 0.3π and 1.3π), which means that the basic flow $\bar{v}$ and $\bar{u}$ are both important at this radial scope. However, when r becomes larger, areas of large and small values of $\Delta C_{g,\theta}$ turn anticlockwise and basically overlap areas of large and small values of wavenumber-1 perturbation flow (e.g., when $r \approx 0.1$, the large and small $\Delta C_{g,\theta}$ are located at about 0.5π and 1.5π), which suggests that the tangential wavenumber-1 perturbation plays a more important role for such conditions. Moreover, the locations of large and small $\Delta C_{g,\theta}$ turn anticlockwise with a continuous increase of r, indicating that the influence of radial flow decreases rapidly with increasing r. As a result, both the tangential wavenumber-1 perturbation flow and the radial basic flow both can increase (decrease) the value of $\Delta C_{g,\theta}$, but the importance of the radial basic flow is only concentrated in areas for smaller r, and $\Delta C_{g,\theta}$ is dominated by the tangential wavenumber-1 perturbation when r becomes larger.

Based on the wave ray equation, Eq. (17), the ratio of $C_{g,r}$ to $C_{g,\theta}$ determines the ray slope of vortex Rossby waves. Distributions of ray slopes in symmetric and asymmetric basic flows are shown in Fig. 8, which indicates that in the symmetric basic flow (Fig. 8a) the ray slope is only associated with the radius, and its distribution is similar to that of the group velocity, with the maximum value occurring at $r = 0.1$. In the asymmetric basic flow (Fig. 8b), the distribution of the ray slope is completely different to that of the group velocity, although the large ray slope still occurs at around $r = 0.1$. Impacts of asymmetry in the basic flow on the wave ray slope are mainly concentrated near the RMW, and the azimuth angle corresponding to the maximum wave ray slope is at around $\theta = 1.13\pi$. Differences between the ray slopes in symmetric and asymmetric basic flows (Fig. 9) indicate that large differences also occur around the RMW, whereas the azimuth angle corresponding to the largest difference varies with the maximum speed of tangential wavenumber-1 perturbation flow and the radial basic flow. It is worth noting that the influence of asymmetry is still important for larger r, and this can explain the reason why the difference between wave rays of asymmetric flow and symmetric flow is great in Fig. 3.

5. Conclusions

In the present study, wave ray theory is applied to investigate the impact of asymmetry in basic flow of typhoons on vortex Rossby waves, including the wave ray path, the group velocity, and the wave ray slope. The major conclusions are as follows:

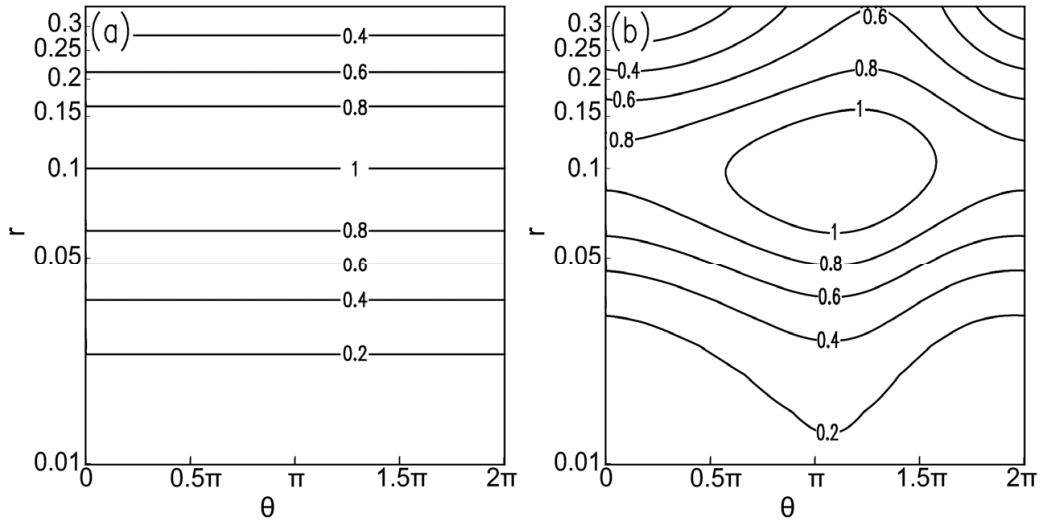

Fig. 8. Distribution of the wave ray slope on the θ–r plane in (a) symmetric and (b) asymmetric basic flow.

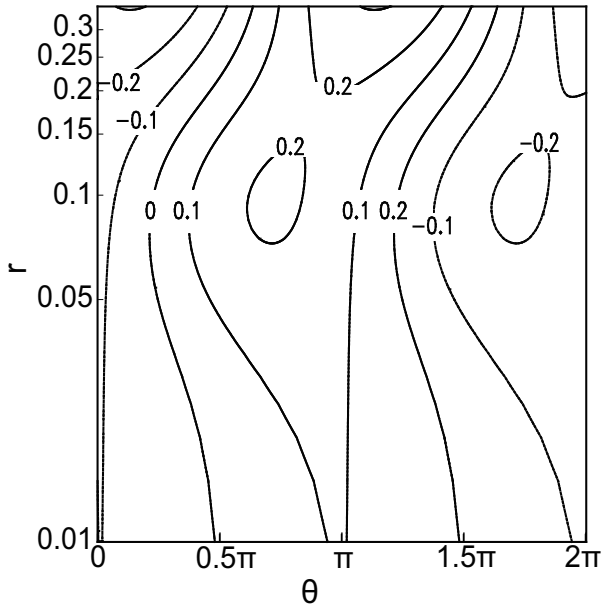

Fig. 9. Differences between wave ray slopes in asymmetric and symmetric basic flows on the θ–r plane.

(1) Compared to symmetric basic flow, the asymmetry in the basic flow will change the ray paths of vortex Rossby waves in typhoons. The wave rays of the asymmetric basic flow are always located outside that of the symmetric basic flow. Stronger asymmetry in the basic flow corresponds to a larger difference between the wave rays in symmetric and asymmetric basic flows. The impacts of the asymmetry in the basic flow on the wave ray path are mainly concentrated in areas for smaller r, and it will diminish generally with increasing r beyond a certain radius.

(2) The asymmetry in the basic flow has substantial impacts on radial and tangential group velocities of vortex Rossby waves. In the asymmetric basic flow, the radial and tangential group velocities change not only with the radius, but also the azimuth angle. The impact of asymmetry in the basic flow on group velocity is mainly concentrated near the RMW. Maximum wave energy propagation speeds along the radial and tangential directions near the RMW are almost equivalent to the maximum speed of tangential basic flow. Both the tangential basic flow and the radial basic flow can affect the group velocities, but the influence of radial basic flow only appears for smaller r, whereas the influence of tangential basic flow can maintain in the whole area we studied.

(3) The asymmetry in the basic flow can change the wave ray slope by affecting the radial and tangential group velocities of vortex Rossby waves, and eventually influence the wave ray path. However, the impact of asymmetry in the basic flow on the wave ray slope is mainly concentrated near the RMW.

Note that the above results are based on vortex Rossby waves on the f-plane; the β-plane and the three-dimensional structure of vortex Rossby waves in asymmetric conditions should be considered in the future.

Acknowledgements. This work was sponsored by the National Natural Science Foundation of China (Grant No. 41430426).

REFERENCES

Anthes, R. A., 1972: Development of asymmetries in a three-dimensional numerical model of the tropical cyclone. *Mon. Wea. Rev.*, **100**, 461–476, https://doi.org/10.1175/1520-0493(1972)100<0461:DOAIAT>2.3.CO;2.

Deng, L. T., S. K. Liu, X. D. Xu, and Z. T. Fu, 2004: The effect of Rossby parameter in vortex Rossby wave. *Journal of Tropical Meteorology*, **20**(5), 483–492, https://doi.org/10.3969/j.issn.1004-4965.2004.05.004. (in Chinese with English abstract)

Hall, J. D., M. Xue, L. K. Ran, and L. M. Leslie, 2013: High-resolution modeling of typhoon Morakot (2009): vortex Rossby waves and their role in extreme precipitation over Taiwan. *J. Atmos. Sci.*, **70**(1), 163–186, https://doi.org/10.1175/JAS-D-11-0338.1.

Huang, R. X., and J. P. Chao, 1980: The linear theory of spiral cloud bands of typhoon. *Scientia Atmospherica Sinica*, **4**(2), 148–158, https://doi.org/10.3878/j.issn.1006-9895.1980.02.06. (in Chinese with English abstract)

Kurihara, Y., 1976: On the development of spiral bands in a tropical cyclone. *J. Atmos. Sci.*, **33**, 940–958, https://doi.org/10.1175/1520-0469(1976)033<0940:OTDOSB>2.0.CO;2.

Liu, S. K., and D. S. Yang, 1980: The spiral structure of the tropical cyclone. *Acta Meteorologica Sinica*, **38**(3), 193–204, https://doi.org/10.11676/qxxb1980.024. (in Chinese with English abstract)

Liu, S. K., and S. D. Liu, 2011: Basic equations of atmospheric motions. *Atmospheric Dynamics*, 2nd ed., S. K. Liu and S. D. Liu, Eds., Peking University Press, Beijing, 39–40. (in Chinese)

Luo, Z. X., and L. S. Chen, 2003: The influence of topography on vortex Rossby waves. *Progress in Natural Science*, **13**(4), 372–377, https://doi.org/10.3321/j.issn:1002-008X.2003.04.007. (in Chinese)

MacDonald, N. J., 1968: The evidence for the existence of Rossby-like waves in the hurricane vortex. *Tellus*, **20**, 138–150, https://doi.org/10.1111/j.2153-3490.1968.tb00358.x.

Montgomery, M. T., and R. J. Kallenbach, 1997: A theory for vortex Rossby-waves and its application to spiral bands and intensity changes in hurricanes. *J. Roy. Meteor. Soc.*, **123**, 435–465, https://doi.org/10.1002/qj.49712353810.

Niu, X. X., 1991: The effect of inertial gravity waves on the occurrence, development and movement of typhoon in unsteady state. *Acta Oceanologica Sinica*, **13**(3), 325–332. (in Chinese)

Qiu, X., Z.-M. Tan, and Q. N. Xiao, 2010: The roles of vortex Rossby waves in hurricane secondary eyewall formation. *Mon. Wea. Rev.*, **138**, 2092–2109, https://doi.org/10.1175/2010MWR3161.1.

Shen, X. Y., J. Ming, and K. Fang, 2007: The properties of wave in typhoon and its numerical simulation. *Scientia Meteorologica Sinica*, **27**(2), 176–186, https://doi.org/10.3969/j.issn.1009-0827.2007.02.009. (in Chinese with English abstract)

Tao, J. J., X. H. Hu, and C. K. Li, 2012: The formation mechanism and change characteristics of the wavenumer-1 vortex Rossby wave in the typhoon. *Acta Meteorological Sinica*, **70**(6), 1200–1206, https://doi.org/10.11676/qxxb2012.101. (in Chinese with English abstract)

Tatehira, R., 1961: Analysis of small precipitation areas and bands,

case study of typhoon "Hellen". *Second Technology Conference of Hurricanes*, Miami, FL, American Meteorology Society, 115–126.

Tepper, M. A., 1958: A theoretical model for hurricane radar bands. *Preprints of 7th Weather Radar Conference*, Miami, FL, American Meteorology Society, 56–65.

Wexler, H., 1947: Structure of hurricanes as determined by radar. *Annals of the New York Academy of Sciences*, **48**(8), 821–845, https://doi.org/10.1111/j.1749-6632.1947.tb38495.x.

Yu, Z. H., 2002: The spiral rain bands of tropical cyclone and vortex Rossby waves. *Acta Meteorologica Sinica*, **60**(4), 502–507, https://doi.org/10.3321/j.issn:0577-6619.2002.04.014. (in Chinese with English abstract)

Zhong, K., J. W. Kang, and Q. P. Yu, 2002: Vortex Rossby waves in hurricane. *Acta Meteorologica Sinica*, **60**(4), 436–441, https://doi.org/10.3321/j.issn:0577-6619.2002.04.006. (in Chinese with English abstract)

Zhong, Z, X.-T. Wang, and J.-S. Zhang, 2007: The possible mechanism on the formation and intensification of the maximum wind core in tropical cyclone. *Asia-Pacific Journal of Atmospheric Sciences*, **43**, 101–110.